Optogenetic stimulation of glutamatergic neurons in the cuneiform nucleus controls locomotion in a mouse model of Parkinson's disease

Maxime Fougère[a], Cornelis Immanuel van der Zouwen[a], Joël Boutin[a], Kloé Neszvecsko[a], Philippe Sarret[a,b,c,d], and Dimitri Ryczko[a,b,c,d,1]

[a]Département de Pharmacologie-Physiologie, Faculté de Médecine et des Sciences de la Santé, Université de Sherbrooke, Sherbrooke, QC J1K 2R1, Canada; [b]Centre de Recherche du Centre Hospitalier, Université de Sherbrooke, Sherbrooke, QC J1K 2R1, Canada; [c]Centre d'Excellence en Neurosciences, Université de Sherbrooke, Sherbrooke, QC J1K 2R1, Canada; and [d]Institut de Pharmacologie de Sherbrooke, Université de Sherbrooke, Sherbrooke, QC J1K 2R1, Canada

Edited by Peter L. Strick, University of Pittsburgh, Pittsburgh, PA, and approved September 7, 2021 (received for review June 13, 2021)

In Parkinson's disease (PD), the loss of midbrain dopaminergic cells results in severe locomotor deficits, such as gait freezing and akinesia. Growing evidence indicates that these deficits can be attributed to the decreased activity in the mesencephalic locomotor region (MLR), a brainstem region controlling locomotion. Clinicians are exploring the deep brain stimulation of the MLR as a treatment option to improve locomotor function. The results are variable, from modest to promising. However, within the MLR, clinicians have targeted the pedunculopontine nucleus exclusively, while leaving the cuneiform nucleus unexplored. To our knowledge, the effects of cuneiform nucleus stimulation have never been determined in parkinsonian conditions in any animal model. Here, we addressed this issue in a mouse model of PD, based on the bilateral striatal injection of 6-hydroxydopamine, which damaged the nigrostriatal pathway and decreased locomotor activity. We show that selective optogenetic stimulation of glutamatergic neurons in the cuneiform nucleus in mice expressing channelrhodopsin in a Cre-dependent manner in Vglut2-positive neurons (Vglut2-ChR2-EYFP mice) increased the number of locomotor initiations, increased the time spent in locomotion, and controlled locomotor speed. Using deep learning-based movement analysis, we found that the limb kinematics of optogenetic-evoked locomotion in pathological conditions were largely similar to those recorded in intact animals. Our work identifies the glutamatergic neurons of the cuneiform nucleus as a potentially clinically relevant target to improve locomotor activity in parkinsonian conditions. Our study should open avenues to develop the targeted stimulation of these neurons using deep brain stimulation, pharmacotherapy, or optogenetics.

Parkinson's disease | cuneiform nucleus | Vglut2 | locomotion | optogenetics

In Parkinson's disease (PD), midbrain dopaminergic (DA) cells are lost, resulting in motor dysfunction, including severe locomotor deficits (e.g., gait freezing, akinesia, and falls) (1). Growing evidence indicates that part of these deficits can be attributed to changes in the mesencephalic locomotor region (MLR) (refs. 2–7; for review, see ref. 8). This brainstem region plays a key role in locomotor control by sending projections to reticulospinal neurons that carry the locomotor drive to the spinal cord in vertebrates (lamprey: refs. 9 and 10; salamander: refs. 11 and 12; and mouse: refs. 13 to 19; for review, see ref. 20). The DA neurons of the substantia nigra pars compacta (SNc) indirectly control MLR activity through the basal ganglia (15, 21, 22). In parallel, the MLR receives direct DA projections from the SNc (23–26) and from the zona incerta (27). The DA innervation of the MLR degenerates in a monkey model of PD (28). Therefore, the loss of DA cells in PD has major effects on MLR activity. In PD, locomotor deficits are associated with MLR cell loss, abnormal neural activity, altered connectivity, and metabolic deficits, likely resulting in a loss of amplification of the locomotor commands (for review, see ref. 8). Accordingly, motor arrests and gait freezing are associated with a decrease in MLR activity in PD (ref. 29; for review, see ref. 8).

One approach to improve locomotor function in PD would be to increase MLR activity. L-DOPA, the gold standard drug used to improve motor symptoms in PD, increases MLR activity and this likely contributes to the locomotor benefits (30). The MLR has been proposed to contribute to the locomotor benefits of deep brain stimulation (DBS) of the subthalamic nucleus (31–33), which has direct and indirect projections to the MLR (refs. 34, 35; for review, see ref. 20). However, the benefits of L-DOPA and subthalamic DBS on locomotor deficits may wane over time, highlighting the need to find new therapeutic approaches (36, 37). Since 2005, the MLR has been explored as a DBS target (38). The results vary, from modest to promising (39, 40). However, the best target in the MLR in PD conditions is not yet identified. The MLR is a heterogeneous structure, with the cuneiform nucleus (CnF) controlling the largest range of locomotor speeds, and the pedunculopontine nucleus (PPN) controlling slow speeds, posture and in some cases locomotor arrests (refs. 15, 17–19; for review, see ref. 20). Human DBS protocols targeted the PPN, but left the

Significance

In Parkinson's disease, alleviating locomotor deficits is a challenge. Clinicians are exploring the deep brain stimulation of the mesencephalic locomotor region, a brainstem region controlling locomotion, but results are mixed. However, the best target in this region in Parkinson's disease remains unknown. Indeed, this region, which comprises the pedunculopontine and cuneiform nuclei, contains different cell types with opposing effects on locomotor output. Here, using mice in which midbrain dopaminergic cells were damaged by a neurotoxin, we demonstrate that optogenetic activation of glutamatergic neurons in the cuneiform nucleus increases locomotion, controls speed, and evokes limb movements similar to those observed during spontaneous locomotion in intact animals. Our study identifies a potentially clinically relevant target to improve locomotor function in Parkinson's disease.

Author contributions: M.F., C.I.v.d.Z., and D.R. designed research; M.F. and J.B. performed research; M.F., C.I.v.d.Z., J.B., and D.R. analyzed data; K.N. and P.S. contributed to methodology; and M.F., C.I.v.d.Z., J.B., K.N., P.S., and D.R. wrote the paper.

The authors declare no competing interest.

This article is a PNAS Direct Submission.

[1]To whom correspondence may be addressed. Email: dimitri.ryczko@usherbrooke.ca.

Published October 20, 2021.

CnF unexplored, despite its major importance in locomotor control in animal research (19, 41, 42). In humans, a recent anatomical analysis of DBS electrode position relative to the pontomesencephalic junction suggests that some of the beneficial effects attributed to the PPN could be due to CnF activation (43).

To add further complexity, three main cell types are present in the MLR: glutamatergic, GABAergic, and cholinergic cells. It is still unknown which cell type is the best target to improve locomotor function in PD conditions. Optogenetic studies uncovered that glutamatergic cells in the CnF play a key role in generating the locomotor drive for a wide range of speeds (15, 17–19). Glutamatergic cells of the PPN control slower speeds (17, 18) and, in some cases, evoke locomotor arrests (18, 44, 45). The GABAergic cells in the CnF and PPN stop locomotion likely by inhibiting glutamatergic cells (15, 17). The role of the PPN cholinergic cells is not resolved, as their activation can increase or decrease locomotion (refs. 15, 17, 18; for review, see ref. 20). Clinically, DBS likely stimulates all cells around the electrode, including the GABAergic cells that stop locomotion, and this could contribute to the variability of outcomes.

Here, we aimed at identifying a relevant target in the MLR to improve the locomotor function in parkinsonian conditions. We hypothesized that the selective activation of CnF glutamatergic neurons should improve locomotor function in a mouse model of PD. We induced parkinsonian conditions in mice by bilaterally injecting into the striatum the neurotoxin 6-hydroxydopamine (6-OHDA), which is well known to damage the nigrostriatal DA pathway and to induce a dramatic decrease in locomotor activity (e.g., refs. 22 and 46). Using in vivo optogenetics in mice expressing channelrhodopsin in a Cre-dependent manner in Vglut2-positive neurons (Vglut2-ChR2-EYFP mice), we show that the photostimulation of glutamatergic neurons in the CnF robustly initiated locomotion, reduced immobility, increased the time spent in locomotion, and precisely controlled locomotor speed. Our results should help in defining therapeutic strategies aimed at specifically activating CnF glutamatergic neurons to improve locomotor function in PD using optimized DBS protocols, pharmacotherapy, or future optogenetic tools for human use.

Results

Striatal 6-OHDA Damages the Striatal DA Innervation and SNc DA Cells. Vglut2-ChR2-EYFP mice were injected bilaterally in the striatum with 6-OHDA to damage the nigrostriatal pathway and induce deficits in locomotor activity similar to those reported in PD (0.2% ascorbic acid, 0.9% NaCl saline solution, 6-OHDA 5 mg/mL, and 1 µL/side). Another group of animals was injected in the striatum with a vehicle (0.2% ascorbic acid, 0.9% NaCl saline solution, and 1 µL/side) (see *Materials and Methods*) (Fig. 1*A*). Striatal 6-OHDA injections significantly decreased the presence of fibers positive for tyrosine hydroxylase (TH; the rate-limiting enzyme for dopamine synthesis) in the striatum, compared to mice injected with vehicle (Fig. 1 *A–E*). The statistical analysis of the optical density of TH labeling in the striatum indicated a −29% decrease in animals injected with 6-OHDA, compared to animals injected with vehicle ($P < 0.001$, t test , and 81.0 ± 2.2 in $n = 6$ vehicle mice versus 57.8 ± 3.5 in $n = 5$ 6-OHDA mice) (Fig. 1*K*). In the SNc, striatal 6-OHDA injections decreased the number of TH^+ cells per centimeters squared by −27% when compared to mice injected with vehicle ($P < 0.05$, t test, and 8,995 ± 656 TH^+ cells/cm^2 in $n = 6$ vehicle mice versus 6,561 ± 531 TH^+ cells/cm^2 in $n = 5$ 6-OHDA mice) (Fig. 1 *F–J*, *L*). When pooling the results from animals injected with vehicle or 6-OHDA, we found a positive linear relationship between the number of TH^+ cells per centimeters squared in the SNc and the striatal TH optical density ($R = 0.70$ and $P < 0.05$; Fig. 1*M*). In a separate analysis, we compared the results obtained in mice injected with vehicle to those obtained in another group of mice without surgery (intact mice), and we found no difference in the striatal TH optical density ($P > 0.05$, t test, and 81.0 ± 2.2 in $n = 6$ vehicle mice versus 86.0 ± 1.6 in $n = 5$ intact mice) and no difference in the number of TH^+ cells per centimeters squared in the SNc ($P > 0.05$, t test, and 8,995 ± 656 TH^+ cells/cm^2 in $n = 6$ vehicle mice versus 9,789 ± 483 TH^+ cells/cm^2 in $n = 6$ intact mice). Altogether, this indicated that the striatal injection of 6-OHDA lesioned the nigrostriatal pathway, while the striatal vehicle injection had no detectable effect on the anatomical integrity of the nigrostriatal pathway.

Striatal 6-OHDA Evokes Locomotor Deficits in the Open-Field Arena. We tracked the locomotor activity from above in the open-field arena using video recordings coupled with deep learning–based analysis (see *Materials and Methods*) (Fig. 2 *A–D*). When comparing locomotor activity during 4.5-min trials before and after bilateral striatal injection of 6-OHDA ($n = 5$ mice and 7 trials per animal per condition), we found a decrease of −91% of time spent in locomotion ($P < 0.01$, paired t test, and 64.5 ± 6.5 before versus 5.9 ± 3.2 s after; Fig. 2*E*), a decrease of −89% in the number of locomotor initiations ($P < 0.01$, paired t test, and 60.7 ± 6.4 versus 6.4 ± 3.2 locomotor initiations; Fig. 2*F*), a decrease of −83% in locomotor speed ($P < 0.01$, paired t test, and 5.1 ± 0.5 versus 0.9 ± 0.2 cm/s; Fig. 2*G*), a decrease of −22% in the duration of the locomotor bouts ($P < 0.05$, paired t test, and 1.1 ± 0.0 versus 0.8 ± 0.1 s; Fig. 2*H*), and a +29% increase of time spent immobile ($P < 0.01$, paired t test, and 205.4 ± 6.5 versus 264.0 ± 3.2 s; Fig. 2*I*).

In comparison, animals injected with vehicle bilaterally in the striatum ($n = 6$ mice) displayed smaller locomotor deficits in the open-field arena (Fig. 2 *E–I*). Importantly, the locomotor deficits were more dramatic in animals injected with 6-OHDA than in those injected with vehicle. In mice injected with 6-OHDA, we found a shorter time spent in locomotion ($P < 0.001$, t test, and 32.5 ± 3.8 in six vehicle mice versus 5.9 ± 3.2 s in five 6-OHDA mice; Fig. 2*E*), a smaller number of locomotor initiations ($P < 0.001$, t test, and 31.5 ± 3.8 versus 6.4 ± 3.2 locomotor initiations; Fig. 2*F*), a slower locomotor speed ($P < 0.001$, t test, and 2.9 ± 0.3 versus 0.9 ± 0.2 cm/s; Fig. 2*G*), a shorter locomotor bout duration ($P < 0.01$, t test, and 1.0 ± 0.0 versus 0.8 ± 0.1 s; Fig. 2*H*), and a longer time spent immobile ($P < 0.001$, t test, and 237.5 ± 3.8 versus 264.0 ± 3.2 s; Fig. 2*I*). All these parameters were similar in the two groups of mice before the injection of 6-OHDA ($n = 5$ mice) or vehicle ($n = 6$ mice) ($P > 0.05$ in all cases, t tests; Fig. 2 *E–I*). Time spent in the center of the arena relative to the duration of the trial was not different before and after 6-OHDA injections ($P > 0.05$, paired t test, and 10.0 ± 2.7 versus 25.1 ± 9.1% of trial time duration), before and after NaCl injections ($P > 0.05$, paired t test, and 7.6 ± 0.9 versus 9.1 ± 2.1%), between the two groups of mice before the injection of 6-OHDA or vehicle ($P > 0.05$, Mann–Whitney rank sum test, and 7.6 ± 0.9 versus 10.0 ± 2.7%), or between the two groups of mice after the injection of 6-OHDA or vehicle ($P > 0.05$, Mann–Whitney rank sum test, and 9.1 ± 2.1 versus 25.1 ± 9.1%).

Next, we examined the relationships between the anatomical integrity of the nigrostriatal pathway and the locomotor deficits in the open-field arena by pooling the results of 11 mice injected in the striatum either with vehicle ($n = 6$ mice) or with 6-OHDA ($n = 5$ mice). We found positive linear relationships between the striatal TH optical density and the following: 1) the time spent in locomotion ($P < 0.01$ and $R = 0.79$; Fig. 2*J*), 2) the number of locomotor initiations ($P < 0.01$ and $R = 0.77$; Fig. 2*K*), 3) the locomotor speed ($P < 0.01$ and $R = 0.76$; Fig.

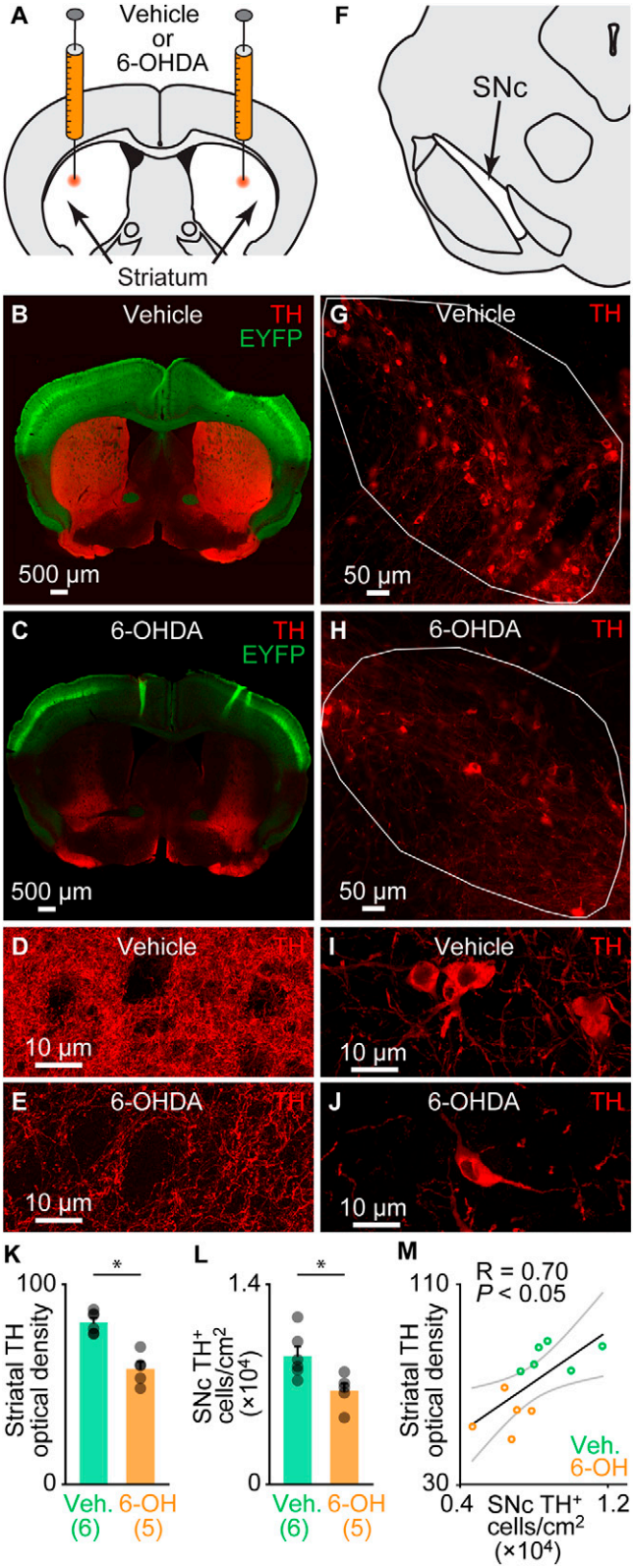

Fig. 1. Bilateral striatal injection of 6-OHDA disrupts the nigrostriatal pathway. (*A*) Schematic illustration of the injection of 6-OHDA in the striatum (5 mg/mL, 1 µL per side; see *Materials and Methods*). (*B* and *C*) Comparison of striatal innervation by TH-positive fibers in a Vglut2-ChR2-EYFP mouse 3 d after bilateral striatal injections of vehicle (see *Materials and Methods*) (*B*) and in another one 3 d after bilateral striatal 6-OHDA injections (*C*). (*D* and *E*) Magnification showing TH immunofluorescence in the striatum of an animal injected with vehicle (*D*) or with 6-OHDA (*E*). (*F*) Schematic illustration of the location of TH-positive neurons in the SNc. (*G* and *H*) Comparison of the presence of the TH-positive cells in the SNc (delineated by the solid white lines), in a mouse injected in the striatum with vehicle (*G*) and another injected with 6-OHDA (*H*). (*I* and *J*) Magnification showing TH immunofluorescence in the SNc of an animal injected with vehicle (*I*) or with 6-OHDA (*J*). (*K*) Bar chart illustrating the optical density of TH immunofluorescence in the striatum of mice injected with vehicle (Veh) versus mice injected with 6-OHDA (6-OH). The number of animals used is indicated between brackets. *$P < 0.05$, *t* test. (*L*) Bar chart illustrating the average bilateral number of TH-positive cells per surface unit in the SNc (two slices counted per mouse; see *Materials and Methods*). *$P < 0.05$, *t* test. (*M*) Relationship between the number of TH-positive cells per surface unit and the striatal TH optical density in the pooled dataset ($n = 11$, including six mice injected with vehicle, green circles, and five injected with 6-OHDA, orange circles). *$P < 0.05$, linear fit. The coefficient of correlation (*R*), its significance (*P*), and the CIs (gray) are illustrated.

2*L*), and 4) the locomotor bout duration ($P < 0.001$ and $R = 0.87$; Fig. 2*M*). We found a negative linear relationship between the striatal TH optical density and the time spent immobile ($P < 0.01$ and $R = 0.79$; Fig. 2*N*).

Altogether, these data indicated that striatal 6-OHDA induced major deficits in locomotor activity in the open-field arena. The small locomotor deficits observed in the animals injected with vehicle are likely due to the surgery since vehicle injection did not disrupt the anatomical integrity of the nigrostriatal pathway (see *Striatal 6-OHDA Damages the Striatal DA Innervation and SNc DA Cells*).

CnF Photostimulation Evokes Locomotion in Vglut2-ChR2-EYFP Mice Lesioned with 6-OHDA. To determine whether the activation of the CnF glutamatergic neurons can increase locomotor activity in PD conditions, we used the Cre-dependent expression of transgenes in Vglut2-Cre mice (47). To determine whether CnF neurons expressed Vglut2 in our mice, we crossed Vglut2-Cre with ZsGreen-lox mice and performed RNAscope experiments in the offspring. We found that 98.7% of CnF cells expressing *ZsGreen* messenger RNA (mRNA) also expressed *Vglut2* mRNA (371/376 cells pooled from $n = 4$ mice; Fig. 3 *A*–*G*).

Next, to activate CnF glutamatergic neurons with optogenetics, we crossed Vglut2-Cre mice with ChR2-EYFP-lox mice to obtain Vglut2-ChR2-EYFP mice (19). The optic fiber was implanted 500 µm above the right CnF, as verified by histology ($n = 11$ mice; Fig. 4 *A*, *B*, and *D*), and we validated that ChR2-EYFP was expressed in the CnF (Fig. 4*C*). Using patch-clamp recordings in brain slices, we previously demonstrated that blue light evoked spikes in MLR neurons at short latency in Vglut2-ChR2-EYFP mice (19).

In animals injected bilaterally in the striatum with 6-OHDA, the nigrostriatal pathway was lesioned (Fig. 1), and significant deficits in locomotor activity were observed (Fig. 2). The optogenetic stimulation of CnF Vglut2 neurons with the 470-nm laser evoked robust increases in locomotor activity in the open-field arena in single-animal data (Fig. 4 *F* and *H*) as well as in the pooled data ($n = 5$ mice; Fig. 4*J*). Statistical analysis indicated that CnF photostimulation increased the time spent in locomotion during stimulation (Fig. 4*L*), the number of locomotor initiations (Fig. 4*N*), the locomotor speed (Fig. 4*P*), and reduced the time spent immobile (Fig. 4*R*). Vglut2-ChR2-EYFP mice injected in the striatum with vehicle also displayed increases in locomotor activity when photostimulated in the CnF with the 470-nm laser (Fig. 4 *E*, *G*, *I*, *K*, *M*, *O*, and *Q*). There was no significant difference in the time spent in the center of the arena during the 10 s of optogenetic stimulation when comparing vehicle and 6-OHDA conditions ($P > 0.05$, Mann–Whitney rank sum test, and 2.6 ± 1.1 versus 7.9 ± 4.0% of the 10 s of optogenetic stimulation). Altogether, these data indicate that the optogenetic stimulation of CnF Vglut2$^+$ neurons can evoke robust increases in locomotor activity in parkinsonian conditions.

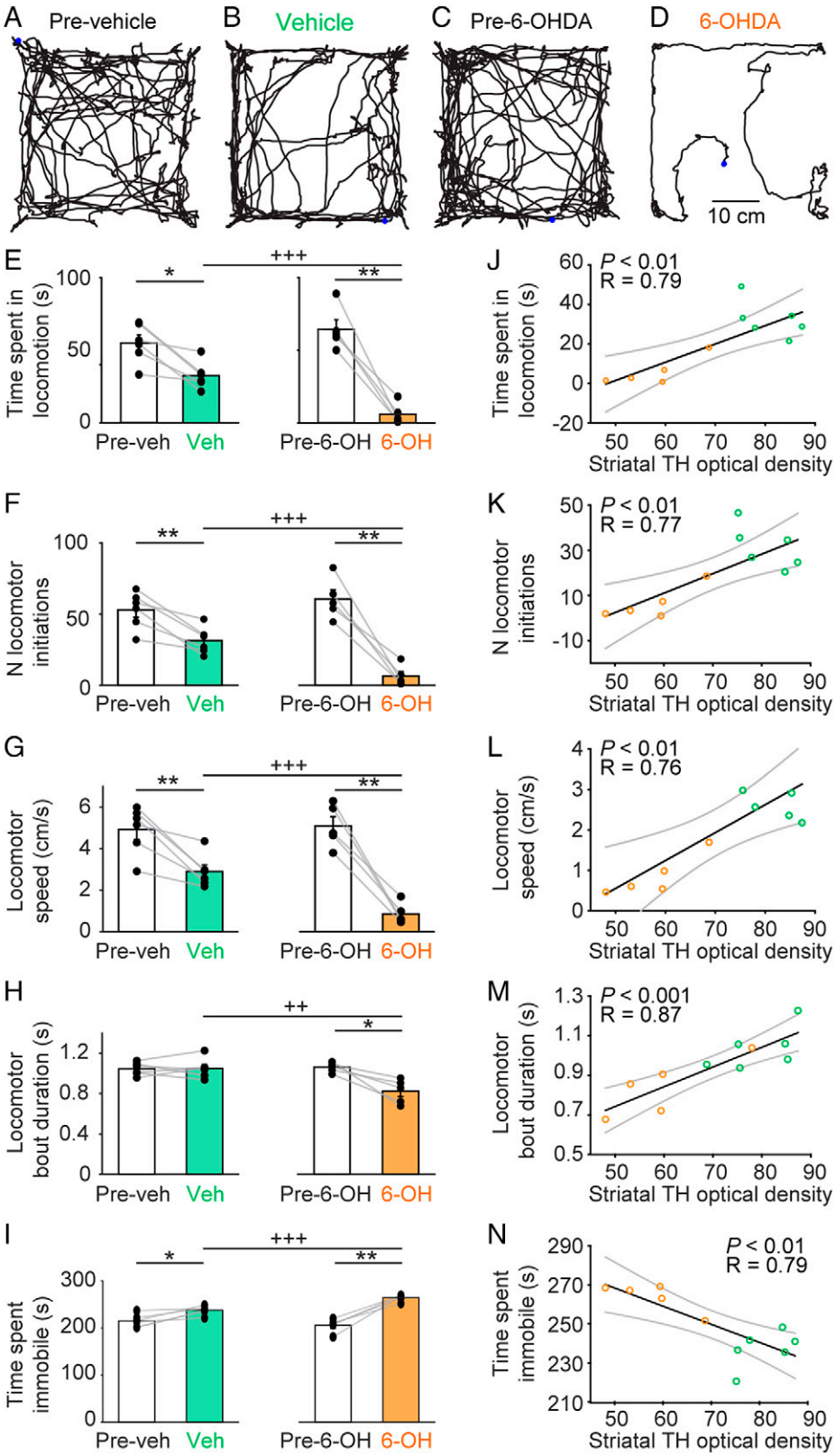

Fig. 2. Bilateral striatal injection of 6-OHDA reduces locomotor activity in the open-field arena. (*A–D*) Locomotor activity recorded from above in the open-field arena during a single trial of 4.5 min before and after bilateral striatal injection of vehicle (*A* and *B*) or 6-OHDA (*C* and *D*). The blue point illustrates the animal's position at the beginning of the trial. (*E–I*) Comparison of locomotor parameters in the open-field arena in six animals injected in the striatum with vehicle (Veh) and five animals injected with 6-OHDA (6-OH) (seven trials recorded per animal). (*E*) Time spent in locomotion (i.e., total time duration during which locomotor speed is higher than 3 cm/s for at least 0.5 s). (*F*) Number (N) of locomotor initiations (i.e., number of times when speed is higher than 3 cm/s for at least 0.5 s). (*G*) Locomotor speed in centimeters per second. (*H*) Locomotor bout duration (i.e., time duration during which locomotor speed is higher than 3 cm/s for at least 0.5 s). (*I*) Time spent immobile, with immobility defined as total time without locomotion. (*J–N*) Linear relationships between the striatal optical density of TH immunofluorescence and the locomotor parameters described in *E–I*. For each fit, the coefficient of correlation (*R*), its significance (*P*), and the CIs (gray) are illustrated. Mice injected with vehicle appear as green circles; those injected with 6-OHDA as orange circles. $^{*}P < 0.05$, $^{**}P < 0.01$, paired tests; $^{++}P < 0.01$, $^{+++}P < 0.001$, *t* tests.

https://doi.org/10.1073/pnas.2110934118

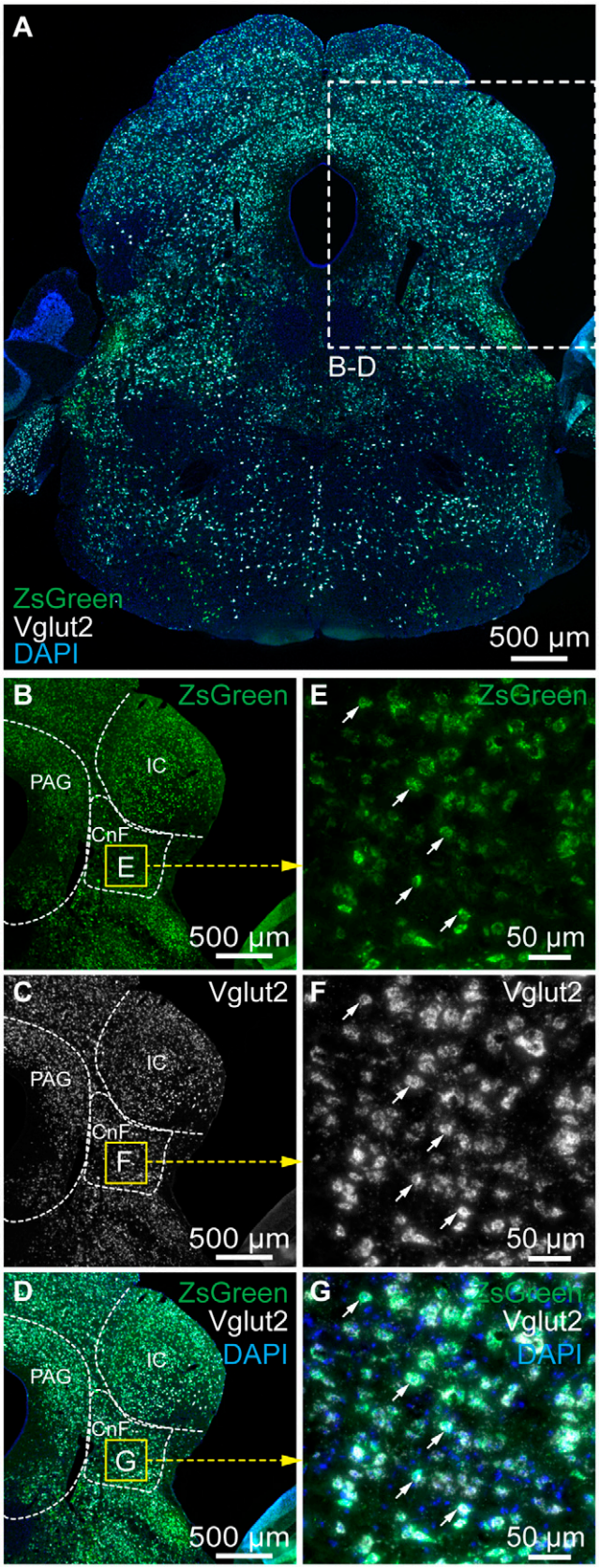

Fig. 3. ZsGreen-positive cells in the cuneiform nucleus express the vesicular glutamatergic transporter 2 *(Vglut2)* mRNA in Vglut2-ZsGreen mice. (*A*) Coronal brainstem slices from a Vglut2-ZsGreen mouse at the level of the cuneiform nucleus, showing the mRNAs of *ZsGreen* (green), *Vglut2* (white) revealed by RNAscope experiments, and a coloration of the nuclear marker DAPI (blue). (*B–D*) Magnification of the slice in *A*, showing the location of the two markers in the cuneiform nucleus. (*E–G*) Magnification of the yellow squares in *B–D*, showing many examples of cells coexpressing *Vglut2* and *ZsGreen* mRNAs (white arrows) in the cuneiform nucleus. CnF, cuneiform nucleus; IC, inferior colliculus; PAG, periaqueductal gray.

CnF Photostimulation Controls Locomotor Speed in Vglut2-ChR2-EYFP Mice Lesioned with 6-OHDA. A major function of the MLR is to control locomotor speed (for review, see ref. 20). Next, we determined whether this key property was still functional in PD conditions. In Vglut2-ChR2-EYFP mice injected bilaterally in the striatum with 6-OHDA, increasing the laser power applied during CnF photostimulation increased the locomotor speed in single-animal data (Fig. 5*B*). Shorter latency to locomotor initiation was associated with increased laser power when expressing laser power as a function of its maximal value per animal in vehicle conditions ($R = -0.69$, $P < 0.05$, Spearman rank order correlation, and $n = 8$ latency values averaged from six mice; Fig. 5*C*) and in 6-OHDA conditions ($R = -0.81$, $P < 0.01$, Spearman rank order correlation, and $n = 10$ latency values averaged from five mice; Fig. 5*D*). We expressed the laser power and speed as a function of their maximal value per animal and found that speed was controlled by laser power in the data pooled from mice lesioned with 6-OHDA (Fig. 5*F*). We found a strong sigmoidal relationship between laser power and locomotor speed in mice lesioned with 6-OHDA ($R = 0.90$, $P < 0.001$, and $n = 5$ mice; Fig. 5*H*). In Vglut2-ChR2-EYFP mice injected in the striatum with vehicle, we also found that increasing laser power increased the locomotor speed in single-animal data (Fig. 5*A*) and in the data pooled from six mice (Fig. 5*E*). We also found in mice injected with vehicle a strong sigmoidal relation between laser power and locomotor speed, expressed as a function of their maximal value per animal ($R = 0.97$ and $P < 0.001$; Fig. 5*G*). To statistically compare the relationships between laser power and speed in mice injected with vehicle or 6-OHDA, we compared the coefficient of correlations of the sigmoidal fits obtained in each animal and found no significant difference ($P > 0.05$, t test, and $R = 0.89 \pm 0.03$ in $n = 6$ vehicle mice, $R = 0.95 \pm 0.02$ in $n = 5$ 6-OHDA mice). Small variations in these relationships from one animal to another could be related to the variable depth or anteroposterior level of the implantation sites (Fig. 4*D*) (19). Overall, this suggests that the lesion of the nigrostriatal pathway did not disrupt the ability of CnF Vglut2$^+$ neurons to control locomotor activity.

Limb Kinematics Evoked by CnF Photostimulation in Vglut2-ChR2-EYFP Mice Lesioned with 6-OHDA. Next, we determined whether normal locomotion was induced by CnF photostimulation. We recorded the hindlimb kinematics in a linear corridor filmed from the side at high speed (see *Materials and Methods* and ref. 19). We compared the limb kinematics by measuring the position of each hindlimb joint (iliac crest, hip, knee, ankle, and metatarsophalangeal [MTP]) and toe over time using DeepLabCut (Fig. 6 *A–D*). In the vehicle group, the angular variations of the hip, ankle, and MTP, as a function of time, were similar during the spontaneous locomotion before vehicle injection and during optogenetic-evoked locomotion after the bilateral striatal injection of vehicle ($P > 0.05$ in all cases, paired t tests; Fig. 6 *A*, *B*, *E*, *G*, *I*, and *J*), except for the knee joint angle that displayed a slightly higher amplitude (+7%) in optogenetic-evoked locomotion after vehicle injection (49.5 ± 2.3 versus $53.3 \pm 2.7°$, $P < 0.01$, paired t test, and $n = 4$ mice; Fig. 6*H*). In the 6-OHDA group, the angular variations of the knee, ankle, and MTP were similar during the spontaneous locomotion before 6-OHDA injection and during optogenetic-evoked locomotion after 6-OHDA injection ($P > 0.05$ in all

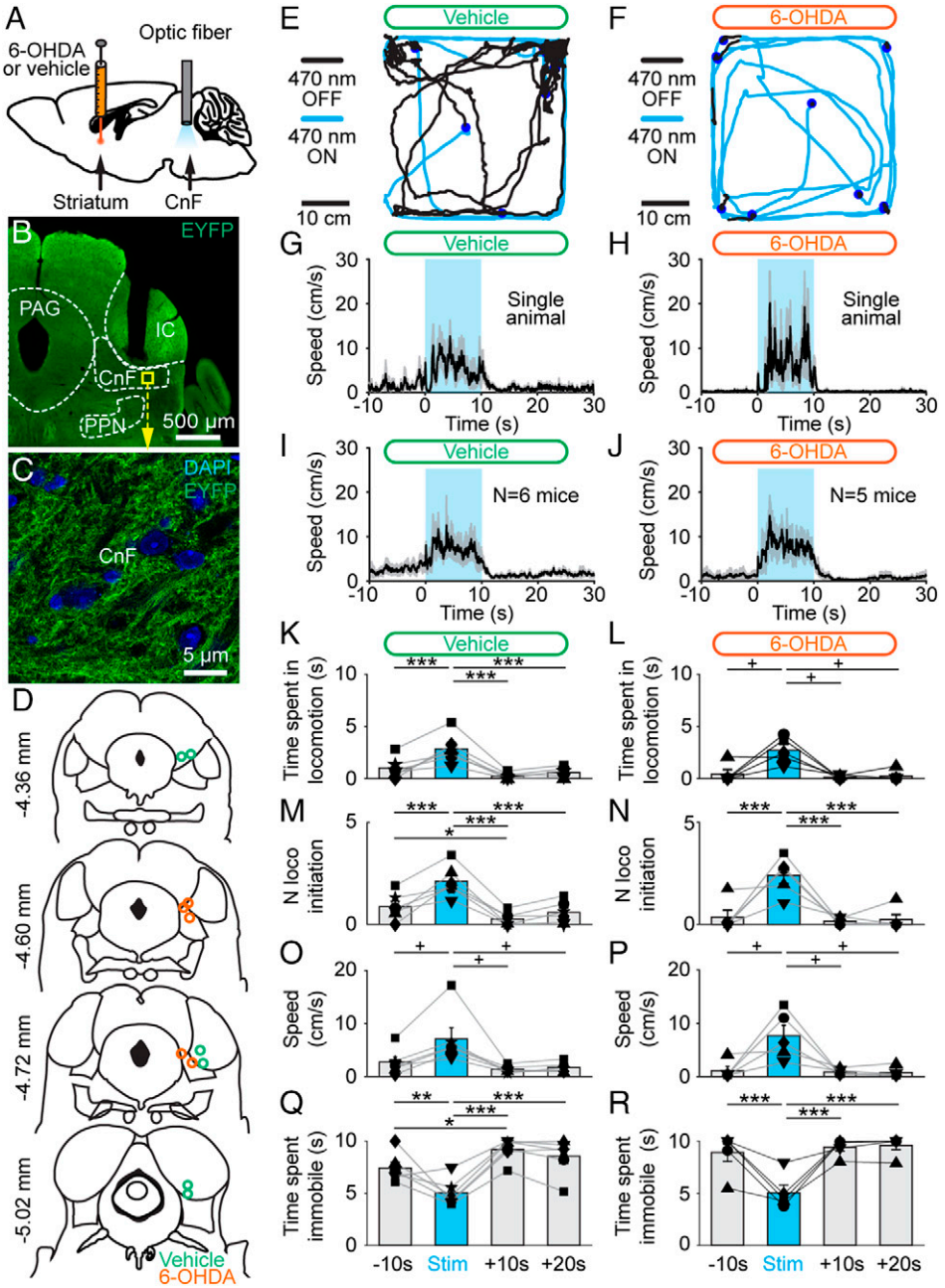

Fig. 4. Optogenetic stimulation of the CnF increases locomotor activity in Vglut2-ChR2-EYFP mice lesioned with 6-OHDA. (*A*) Vglut2-ChR2-EYFP mice were either injected in the striatum with vehicle or 6-OHDA (see *Materials and Methods*) and implanted ~500 µm above the right CnF with an optic fiber. After 3 d, the effects of optogenetic stimulation of the CnF were tested in the open-field arena. (*B*) Photomicrograph showing the position of the optic fiber right above the CnF. (*C*) Magnification of the yellow square in *B*, showing the expression of ChR2-EYFP at the level of the CnF. IC, inferior colliculus; PAG, periaqueductal gray; PPN, pedunculopontine nucleus. (*D*) Location of the optic fibers after the histology of mice injected in the striatum with vehicle (green circles) or 6-OHDA (orange circles). (*E* and *F*) Raw data showing the effects of CnF optogenetic stimulation with a 470-nm laser in a mouse injected in the striatum with vehicle (*E*) (10 s train, 20 Hz, 10 ms pulses, and 5% of laser power), or with a 470-nm laser in a mouse injected in the striatum with 6-OHDA (*F*) (10% of laser power). (*G* and *I*) Locomotor speed (mean ± SEM) before, during, and after a 10-s optogenetic stimulation (onset at $t = 0$ s) with a 470-nm laser in a single animal (*G*) (5% of laser power) or in a pool of six animals injected in the striatum with vehicle (*I*) (10 stimulations per animal and 5 to 20% of laser power). (*H* and *J*) Locomotor speed (mean ± SEM) before, during, and after a 10-s optogenetic stimulation (onset at $t = 0$ s) with a 470-nm laser in a single animal (*H*) (10% of laser power) or in a pool of five animals injected in the striatum with 6-OHDA (*J*) (10 stimulations per animal and 5 to 20% of laser power). (*K*–*R*) Evolution of locomotor parameters before (−10 to 0 s), during (0 to 10 s), and after (10 to 20 s and 20 to 30 s) optogenetic stimulation of the CnF with a 470-nm laser in six animals injected in the striatum with vehicle (*K*, *M*, *O*, and *Q*) and in five animals injected with 6-OHDA (*L*, *N*, *P*, and *R*). $^{*}P < 0.05$, $^{**}P < 0.01$, $^{***}P < 0.001$, Student–Newman–Keuls test after a one-way ANOVA for repeated measures ($P < 0.001$ in *K*, *M*, *N*, *Q*, and *R*). $^{+}P < 0.05$, Student–Newman–Keuls test after a Friedman repeated measures ANOVA on ranks ($P < 0.05$ in *L* and *P*; $P < 0.01$ in *O*).

cases, paired *t* tests; Fig. 6 *C*, *D*, *F*, and *H*–*J*), except for the hip joint angle that displayed a higher amplitude (+38%) in optogenetic-evoked locomotion after 6-OHDA injection (35.1 ± 1.8 versus 48.7 ± 2.9°, $P < 0.05$, paired *t* test, and $n = 5$ mice; Fig. 6*G*). When comparing vehicle and 6-OHDA groups during spontaneous locomotion prior to intracerebral injections,

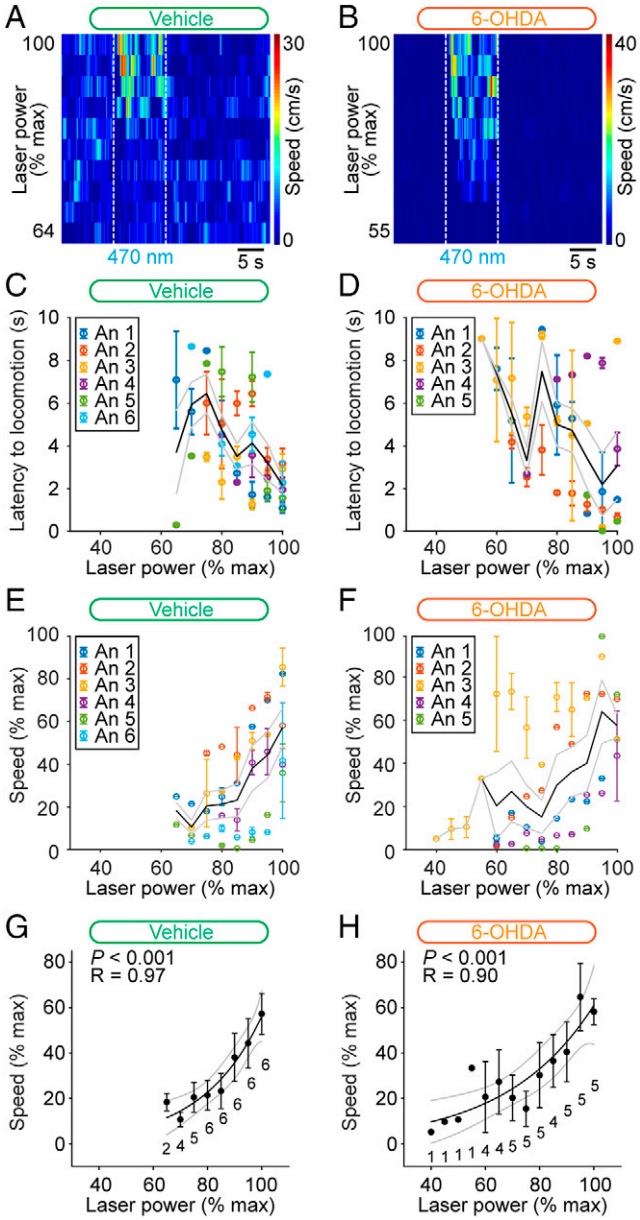

Fig. 5. Control of speed by glutamatergic neurons of the CnF in Vglut2-ChR2-EYFP mice lesioned with 6-OHDA. (*A* and *B*) Color plots illustrating increases in locomotor speed in the open-field arena during optogenetic stimulation of the CnF in an animal injected in the striatum with vehicle (*A*) (3.2 to 5.0% of laser power) or with 6-OHDA (*B*) (5.5 to 10.0% of laser power). (*C* and *D*) Latency to locomotor initiation as a function of laser power (vehicle: 3.2 to 15.5% of laser power and 6-OHDA: 4.5 to 20.0% of laser power). Each dot represents the latency (mean ± SEM) measured during one to three trials. Laser power was normalized as a function of its maximal value per animal (% max) with a bin size of 5%. The average latency (solid black line) and the SEM (gray solid lines) are illustrated. The data from each animal (An) are illustrated with a different color. (*E* and *F*) Locomotor speed (0.3 to 23.5 cm/s in *E* and 0.2 to 30.9 cm/s in *F*) as a function of laser power (vehicle: 3.2 to 15.5% of laser power and 6-OHDA: 3.8 to 20.0% of laser power). Each dot represents the speed (mean ± SEM) measured during one to three trials. Speed and laser power were normalized as a function of their % max with a bin size of 5%. The average speed (solid black line) and the SEM (gray solid lines) are illustrated. The data from each animal are illustrated with a different color. (*G* and *H*) Relationships between locomotor speed (mean ± SEM and bin width 5%) and laser power in the same animals shown in *E* and *F*. For each bin, the number of animals is indicated below the data point. The data followed a sigmoidal function, both in the six animals injected in the striatum with vehicle (*G*) (solid black line, $R = 0.97$, and $P < 0.001$) and in the five animals injected with 6-OHDA (*H*) (solid black line, $R = 0.90$, and $P < 0.001$). For each fit, the coefficient of correlation (*R*), its significance (*P*), and the CIs (gray) are illustrated.

hip, ankle, and MTP angular variations were similar ($P > 0.05$ in all cases, *t* tests, or Mann–Whitney rank sum tests; Fig. 6 *A*, *C*, *E–G*, *I*, and *J*), except for the knee joint angle that showed a higher amplitude (+16%) in the 6-OHDA group (49.5 ± 2.3 versus 57.7 ± 0.9°, $P < 0.01$, *t* test; Fig. 6*H*). Importantly, when comparing limb kinematics during locomotion evoked by optogenetic stimulation in mice injected with vehicle ($n = 4$ mice) or with 6-OHDA ($n = 5$ mice), no difference was found in the angular variations of the hip, knee, ankle, or MTP ($P > 0.05$ in all cases, *t* tests; Fig. 6 *G–J*). Altogether, this indicated that, in parkinsonian conditions, the limb kinematics during locomotion evoked by the optogenetic stimulation of CnF Vglut2$^+$ neurons were largely similar to those recorded during the spontaneous locomotion before lesion.

Discussion

In the present study, we found that the optogenetic stimulation of glutamatergic (Vglut2$^+$) neurons in the CnF increases locomotor activity in a 6-OHDA–based mouse model of PD. Bilateral striatal injection of 6-OHDA in Vglut2-ChR2-EYFP mice damaged the TH-positive innervation of the striatum and damaged SNc DA cells. This was associated with major deficits in locomotor activity in the open-field arena. The optogenetic activation of Vglut2$^+$ neurons in the CnF increased the number of locomotor initiations, reduced the time spent immobile, and locomotor speed was precisely controlled by laser power in mice injected in the striatum with 6-OHDA, as in mice injected with vehicle. The deep learning-based analysis of locomotor movements indicated that limb kinematics evoked by optogenetic stimulation in mice lesioned with 6-OHDA were close to those recorded before lesion. Our study shows that the brainstem locomotor circuits downstream of the midbrain DA cells remain functional despite the dramatic decrease in locomotor activity after 6-OHDA lesion. This indicates that CnF Vglut2$^+$ neurons are likely a relevant target to improve locomotor function in PD conditions.

Targeting CnF Neurons. Although we cannot completely rule out the partial recruitment of Vglut2$^+$ neurons of the PPN or other neighboring structures such as the periaqueductal gray, our results indicate that the Vglut2$^+$ neurons we stimulated are most likely located in the CnF. At the behavioral level, the precise control of speed in freely moving mice that we report here (Fig. 5) is the hallmark of successful activation of glutamatergic neurons in the CnF (15, 17–19). The control of locomotor speed exerted by PPN glutamatergic neurons appears to be less robust than that exerted by CnF ones (17, 18), making their recruitment unlikely here. We did not record any decelerated locomotor rhythms or locomotor stops that were reported to be induced by the activation of glutamatergic PPN neurons in certain cases (18, 44, 45). Limb kinematics were largely normal during CnF stimulation, consistent with our observations in nonparkinsonian animals (19). Future studies should investigate whether subtle differences occur during subparts of the locomotor cycle, since the activation of CnF Vglut2$^+$ neurons increases flexor activity during swing and extensor activity during stance (18). Future studies should also determine whether coupling CnF stimulation with increased DA transmission (apomorphine challenge) would have a synergistic or additive effect on locomotor performance. Whether the behavioral effects evoked by CnF Vglut2$^+$ neuron activation are similar in males

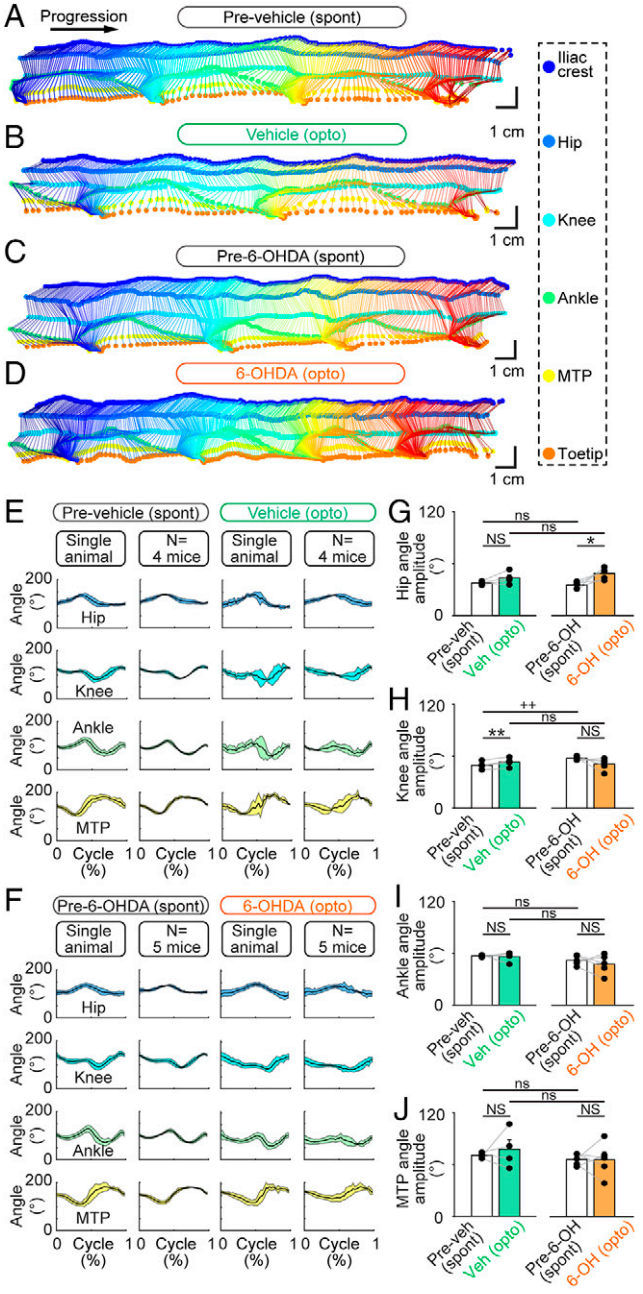

Fig. 6. Hindlimb kinematics evoked by optogenetic stimulation of the CnF in Vglut2-ChR2-EYFP mice lesioned with 6-OHDA. (*A–D*) The movements of six hindlimb joints were tracked from the side at 300 fps in a linear corridor during spontaneous locomotion (spont) before the striatal injection of vehicle (*A*) or 6-OHDA (*C*), and during optogenetic-evoked locomotion (opto) after vehicle injection (*B*) (6.4% of laser power) or 6-OHDA (*D*) (30% of laser power). (*E* and *F*) The joint angles at the hip, knee, ankle, and MTP joint levels were calculated frame by frame. The cycle was defined as the time duration between two consecutive touchdowns of the MTP. A speed threshold of 9 cm/s was used to define the transitions between swing and stance phases. For single-animal data, joint angles (mean ± SD) were plotted for a normalized locomotor cycle during spontaneous locomotion before vehicle (*E*) (31 steps) or before 6-OHDA injection (*F*) (30 steps) and during optogenetic-evoked locomotion after striatal vehicle injection (*E*) (8 steps and 6.4% of laser power) or after striatal 6-OHDA injection (*F*) (32 steps and 10% of laser power). For the pooled data, joint angles (mean ± SD) were plotted for a normalized locomotor cycle during spontaneous locomotion before vehicle injection (*E*) (31 to 39 steps per animal) or before 6-OHDA injection (*F*) (28 to 34 steps per animal) and during optogenetic-evoked locomotion after vehicle injection (*E*) (3 to 19 steps per animal and 5.2 to 20.0% of laser power) and during optogenetic-evoked locomotion after 6-OHDA injection (*F*) (3 to 32 steps per animal and 5 to 30% of laser power). (*G–J*) Comparison of the amplitude of the hip (*G*), knee (*H*), ankle (*I*), and MTP (*J*) angles during spontaneous locomotion before vehicle (Veh) or 6-OHDA (6-OH) injection and during optogenetic-evoked locomotion after vehicle or 6-OHDA injection (vehicle, $n = 6$ mice and 6-OHDA, $n = 5$ mice). NS: not significant, $P > 0.05$, $^{*}P < 0.05$, $^{**}P < 0.01$, paired t tests; ns: not significant, $P > 0.05$, $^{++}P < 0.01$, t test, or Mann–Whitney rank sum test.

and females remains to be examined, although no difference has been reported (17–19).

At the anatomical level, we carefully verified that the optic fiber tips were located in or above the CnF (Fig. 4*D*), as in recent studies targeting the same nucleus (17–19). The light that could spread down to the PPN would be limited, as we estimated that with the highest laser power value used in the present study, ~98% of irradiance is lost at 1 mm from the tip of the optic fiber (18, 48). The location of the activated CnF Vglut2^{+} neurons should be determined by future studies using c-Fos (49).

Targeting Glutamatergic Neurons. We likely stimulated specifically CnF glutamatergic neurons, as ~99% of ZsGreen-positive cells in the CnF of Vglut2-ZsGreen mice expressed *Vglut2* mRNA (Fig. 3). This is consistent with the fact that *Vglut2* is specifically expressed in neurons (50) and with our observation in Vglut2-ZsGreen mice that the vast majority of ZsGreen positive cells are immunopositive for the neuronal marker NeuN (19, 51). Therefore, CnF GABAergic neurons, which decrease locomotor activity when activated (15, 17), were likely not recruited in our study.

Clinical Relevance. Although 6-OHDA does not mimic the chronic degeneration seen in PD, it is useful for the preclinical evaluation of potential interventions in PD (52). In the present study, although we cannot rule out the underestimation of our 6-OHDA–evoked lesions, the anatomical damages to the nigrostriatal pathway appear lower than those reported in PD. Nonetheless, the damages were sufficient to evoke motor deficits.

The main message of the present study is that increasing the activity of glutamatergic (Vglut2^{+}) neurons in the CnF is a relevant approach to improve locomotor function in PD conditions. Since 2005, the MLR has been explored as a DBS target (38) to improve locomotor function in PD, but the results remain mixed (for review, see refs. 39, 40, and 53). One possible reason is that DBS protocols focused on the PPN but left the CnF largely unexplored, despite the major role of the CnF in locomotor control in mammals (refs. 14–19; for review, see refs. 20 and 41). Historically, the MLR was discovered functionally using electrical stimulation in a region encompassing the CnF and the PPN in cats (ref. 54; for review, see ref. 20). In humans, the careful analysis of DBS electrode position relative to the pontomesencephalic junction revealed that patients in whom DBS was most effective against gait freezing had their electrodes located in or around the CnF (43). Future clinical studies should evaluate the effects of CnF DBS on locomotor function, and a first clinical trial is currently exploring this avenue [NCT04218526 (55, 56)].

Future studies should also aim at understanding how to specifically control glutamatergic (Vglut2^{+}) neurons in the CnF using clinically relevant approaches, such as DBS or pharmacological agents. 6-OHDA mice with implanted DBS stimulators are increasingly used to study the effects of stimulation parameters (57) and to visualize the neurons activated using calcium imaging (58) or electrophysiological recordings of optogenetically tagged neurons (59). One possibility would be to consider the electrophysiological properties of CnF glutamatergic neurons to optimize DBS protocols. Most CnF glutamatergic neurons (86% of Vglut2^{+} cells) have homogeneous properties,

whereas PPN glutamatergic neurons are more heterogeneous (44). CnF glutamatergic neurons display membrane potential oscillatory properties in the 20 to 40 Hz range, whereas PPN glutamatergic neurons are in the 10 to 20 Hz (44). Low electrical stimulation frequencies are needed to gently activate MLR neurons and induce locomotion in animal research [15 to 50 Hz in cats (49, 54), 50 Hz in rats (60), 20 to 50 Hz in pigs (42), and 5 to 10 Hz in lampreys and salamanders (9–11)]. Therefore, clinically, the higher stimulation frequencies (50 to 140 Hz) used to disrupt the abnormal ongoing rhythmic activity in the subthalamic nucleus should be avoided in the MLR (e.g., refs. 61 and 62). A second possibility would be to use pharmacological agents designed to preferentially control the activity of CnF glutamatergic neurons. The team of Garcia-Rill reported that histone deacetylases modulate the electrophysiological activity of PPN neurons in brain slices and PPN oscillations in vivo (63, 64). In the future, an alternative to DBS or pharmacological agents could be to develop the use of optogenetics to recruit genetically defined cell types in humans (65). Two ongoing clinical trials aim at improving visual function in retinis pigmentosa using optogenetics (NCT03326336 and NCT02556736).

An interesting aspect relative to targeting CnF glutamatergic neurons is that their activation should not prevent adaptable navigation through the integration of environmental cues. We recently showed that freely behaving mice can brake and turn during optogenetic stimulation of CnF glutamatergic neurons (19), and this observation holds true in PD animals (Fig. 4 *E* and *F*). This is consistent with the recent demonstration that separate reticular circuits control speed and turning (66–68). Another behavioral aspect that we report here is the absence of difference in the time spent exploring the center of the open-field arena during CnF stimulation, suggesting no change in anxiety-like behaviors (69). Alternative measures should be used to confirm this, since the akinetic state of 6-OHDA animals influences the time spent in or out of the center of the arena.

CnF Vglut2$^+$ Neurons in Humans. The presence of glutamatergic and GABAergic neurons in the human CnF has been described using immunohistochemistry (36). The presence of *Vglut2* mRNA has been demonstrated in the human PPN and CnF using in situ hybridization (36). It is well established that cholinergic neurons degenerate in the PPN (2–5, 7). A recent anatomical study reported that some noncholinergic neurons are also lost in the PPN and CnF in PD, but the status of CnF glutamatergic neurons remains to be studied in detail (36). A key aspect will be to determine whether targeting CnF glutamatergic neurons improves locomotion when the benefits of L-DOPA and subthalamic DBS have worn off (37, 70). In this regard, it is particularly interesting to underline the preliminary but promising results of a prospective pilot trial performed in Miami, where a patient with severe freezing of gait refractory to L-DOPA therapy showed improvement in locomotor function after bilateral DBS of the CnF (56). This suggests that enough glutamatergic neurons remain responsive in the CnF in parkinsonian conditions to activate downstream locomotor circuits. The targeted activation of Vglut2$^+$ neurons in the CnF could also be relevant to improve locomotor function in progressive supranuclear palsy, an atypical parkinsonism (71, 72).

Conclusion

Our work indicates that increasing the activity of CnF glutamatergic (Vglut2$^+$) neurons is a relevant approach to improve the locomotor function in PD conditions. Future studies should aim at controlling these neurons using pharmacotherapy, optimized DBS protocols, optogenetic or chemogenetic tools to improve locomotor control and allow smooth navigation in PD conditions.

Materials and Methods

Ethics Statement. All procedures were in accordance with the guidelines of the Canadian Council on Animal Care and were approved by the animal care and use committees of the Université de Sherbrooke. Care was taken to minimize the number of animals used and their suffering.

Animals. We used Vglut2-ires-Cre knock-in mice (Jackson Laboratories, No. 028863, C57BL/6J) (47), ChR2-EYFP-lox mice (Ai32 mice, Jackson Laboratory, No. 024109, and B6.Cg-*Gt(ROSA)26Sor*$^{tm32(CAG-COP4*H134R/EYFP)Hze}$/J) (73), and ZsGreen-lox mice (Ai6 mice, Jackson Laboratory, and No. 007906, B6.Cg-*Gt(ROSA)26Sor*$^{tm6(CAG-ZsGreen1)Hze}$/J) (73). Homozygous Vglut2-ires-Cre knock-in mice were crossed with homozygous ChR2-EYFP-lox mice to obtain double heterozygous Vglut2-ChR2 mice. Homozygous Vglut2-ires-Cre knock-in mice were crossed with homozygous ZsGreen-lox mice to obtain double heterozygous Vglut2-ZsGreen-lox mice. Mice were genotyped as previously described (19, 51). Animals had ad libitum access to food and water, with lights on from 6 AM to 8 PM. Vglut2-ChR2-EYFP mice used for in vivo experiments were 22 to 46 wk old at time of use (five males and six females). Vglut2-ZsGreen mice used for RNAscope experiments were 5 to 8 wk old (four females), and those used for immunofluorescence control experiments were 6 to 18 wk old (five males and one female).

PD Model. The neurotoxin 6-OHDA was successfully used in mice to ablate DA neurons and evoke locomotor deficits resembling those reported in PD, including the decreased number of locomotor initiations (22), increased freezing frequency (22), or akinesia (46). The mice received 30 min prior to 6-OHDA (or vehicle) injection, a systemic injection of desipramine to protect the noradrenergic and serotoninergic systems (25 mg/kg and 300 μL, intraperitoneal injection) (74). Then , mice were anesthetized using isoflurane (induction: 5% and 500 mL/min; maintenance: 1.5 to 2.5% and 100 mL/min) delivered with a SomnoSuite (Kent Scientific) and placed in a Robot Stereotaxic instrument coupled with StereoDrive software (Neurostar). Two holes were drilled in the cranium, and a 10-μL Hamilton syringe locked into the Robot Stereotaxic instrument was used to inject bilaterally in the striatum either 6-OHDA (0.2% ascorbic acid, 0.9% NaCl saline solution, 6-OHDA 5 mg/mL, and 1 μL/side) or the vehicle (0.2% ascorbic acid, 0.9% NaCl saline solution, and 1 μL/side) (22, 74). The syringe needle was lowered at +0.50 mm anteroposterior, ±1.50 mm mediolateral, and −3.00 mm dorsoventral relative to bregma. The compound injected was delivered at a rate of 0.2 μL/min. The syringe was left in place for 5 min before being removed. The scalp incision was sutured, and antibiotics were applied locally. The animals were tested 3 d after 6-OHDA injection when the DA cells have degenerated, and locomotor deficits are observed (22, 46).

Optic Fiber Implantation. The procedure was as previously reported (19). Briefly, mice were anesthetized using isoflurane (induction: 5% and 500 mL/min; maintenance: 1.5 to 2.5% and 100 mL/min) delivered with a SomnoSuite (Kent Scientific). Mice were placed in a Robot Stereotaxic instrument coupled with StereoDrive software (Neurostar). An incision was made on the scalp, a hole was drilled in the cranium, and a fiber (200 mm core and 0.22 numerical aperture, Thorlabs) held in a 5-mm ceramic or stainless steel ferrule was placed 500 μm above the right CnF at −4.70 to -4.75 mm anteroposterior, +1.15 mm mediolateral, and −2.40 mm dorsoventral relative to bregma (17–19). The ferrule was secured on the cranium using two 00-96 × 1/16 mounting screws (HRS Scientific) and dental cement (A-M Systems). The scalp incision was sutured, and antibiotics were applied locally.

In Vivo Optogenetic Stimulation. The procedure was as previously reported (19). Briefly, the implanted optic fiber was connected to a 470-nm laser (Ikecool) using a pigtail rotary joint (Thorlabs). The laser was driven with a Grass S88X to generate the stimulation trains [10 s trains, 10 ms pulses, and 20 Hz (17–19)]. To visualize optogenetic stimulation, a copy of the stimulation trains was sent to a small (diameter 0.5 cm), low-power (0.13 W) red light-emitting diode (LED) coupled with a 120 MΩ resistance (19). The LED was placed in the field of view of the camera placed above the open field. The 470-nm laser was adjusted to 3.2 to 30.0% of laser power. The corresponding power measured at the fiber tip with a power meter (PM100USB, Thorlabs) was 0.1 to 41.2 mW. We estimated irradiance as a function of distance from the optic fiber using a model provided by the Deisseroth Laboratory, based on measurements in brain tissues (https://web.stanford.edu/group/dlab/cgi-bin/graph/chart.php; see also refs. 18 and 48). We previously provided evidence that the evoked locomotor responses are specific to blue light in Vglut2-ChR2-EYFP mice, since replacing the blue laser by a red one (589 nm) does not evoke any locomotor response (19).

Open-Field Locomotion. The procedure was as previously reported (19). Briefly, locomotor activity was filmed from above in a 40 × 40 cm open-field arena at 30 frames per second (fps) using a Canon Vixia HF R800 camera. To measure spontaneous locomotor activity before and after intracerebral injection of the vehicle or 6-OHDA, locomotor activity was recorded during trials of 4.5 min. To measure the effects of optogenetic stimulation, locomotor activity was recorded during trials of 15 min, during which 10 stimulation trains were delivered every 80 s at various laser powers. Video recordings were analyzed with DeepLabCut to track user-defined body parts (75–77) and a custom MATLAB script (MathWorks) (19). We tracked the body center positions, the corners of the arena for distance calibration, and the small LED to detect optogenetic stimulations. Timestamps were extracted using Video Frame Time Stamps (MATLAB File Exchange). Body center positions and timestamps were used to calculate locomotor speed. Time spent in the center of the arena (a 20 × 20 cm square) was measured in some experiments. Body center positions were excluded if their detection likelihood by DeepLabCut was <0.8, if they were outside of the open-field arena, or if body center speed exceeded the maximum locomotor speed recorded in mice [334 cm/s (78)].

Limb Kinematics. The procedure was as previously reported (19). Briefly, to label hindlimb joints, mice were anesthetized, the hindlimb was shaved, and ~2-mm white dots were drawn on the iliac crest, hip, knee, ankle, MTP joints, and toe tip using a fine-tip, oil-based paint marker (Sharpie). After 20 min of recovery from anesthesia, mice were placed in a 1-m-long, 8-cm wide transparent corridor. Hindlimb kinematics were recorded at 300 fps from the side using a high-speed Genie Nano Camera M800 camera (Teledyne DALSA) coupled to a computer equipped with Norpix Streampix software (1stVision). For distance calibration, four markers (diameter 0.5 cm) were distributed 5 cm apart in the field of view of the camera. To detect optogenetic stimulation, an LED that received a copy of the stimulation trains was placed in the field of view of the camera. Animals were recorded during optogenetic-evoked locomotion and during the spontaneous locomotion evoked by a gentle touch of the animal's tail or a gentle air puff generated by a small air bulb.

The positions of the joints and toe tip were detected using DeepLabCut. A moving average of the MTP speed was used to determine the stance and swing phases by detecting the touchdown and lift-off times with a speed threshold of 9 cm/s and a minimum of 14 frames above threshold for the lift-off detection (19). The joint positions were used to extract the angles of the hip, knee, and ankle joints. The angular variations as a function of time were normalized to step cycle duration using MTP touchdown times as a reference (79).

Frames were excluded from the analysis if the MTPs or any limb joints or the toe tip had a detection likelihood by DeepLabCut that was <0.8, if any paw's or joint's speed exceeded 400 cm/s (i.e., maximum locomotor speed of a mouse with a 20% margin to account for increased speed of individual body parts), or if the distance between two adjacent joints was >2.3 cm (i.e., length of the tibia in wild-type mice) (19).

DeepLabCut Networks. The networks used were the same as those described in ref. 19. Briefly, for the analysis of locomotion in the open-field arena, we labeled the body center, the corners of the arena, and the LED to visualize optogenetic stimulation. We used a ResNet-50–based neural network (80, 81), with default parameters for 1,030,000 training iterations. We validated with one shuffle and found that the test error was 2.28 pixels and the train error 1.85 pixels (19).

For limb kinematics analysis, we labeled the five joints and the toe tip, four distance calibration markers, and the low-power LED to visualize optogenetic stimulation. We used a ResNet-50–based neural network (80, 81), with default parameters for 1,030,000 training iterations and one refinement of 1,030,000 iterations. We validated with one shuffle and found that the test error was 2.03 pixels and the train error 1.87 pixels (19).

Histology. Procedures were as previously reported (19, 51). Briefly, mice were anesthetized using isoflurane (5% and 2.5 L/min) and transcardially perfused with 30 to 50 mL phosphate buffer solution (0.1 M) containing 0.9% of NaCl (PBS) (pH = 7.4), followed by 50 mL PBS solution containing 4% (weight/volume) paraformaldehyde (PFA; 4%). The postfixation of the brains was performed for 24 h in a solution of PFA 4%. Brains were incubated in a phosphate buffer containing 20% (weight/volume) sucrose for 24 h before histology. Brains were snap frozen in methylbutane (−45 °C ± 5 °C) and sectioned at −20 °C in 40-μm-thick coronal slices using a cryostat (Leica CM 1860 UV). Floating sections at the level of the MLR, striatum, and SNc were collected under a Stemi 305 stereomicroscope (Zeiss) and identified using the mouse brain atlas of Franklin and Paxinos (82).

Immunofluorescence. The procedure was as previously reported (19, 51). All steps were carried out at room temperature unless stated otherwise. The sections were rinsed three times during 10 min in PBS and incubated during 1 h in a blocking solution containing 5% (volume/volume) of normal donkey serum and 0.3% Triton X-100 in PBS. The sections were incubated during 48 h at 4 °C in a blocking solution containing the primary antibody against TH (rabbit anti-TH, Millipore AB152, lots 2795024 and 3114503 [1:1,500]; RRID: AB_390204) and gently agitated with an orbital shaker. Then, the sections were washed three times in PBS and incubated during 4 h in a blocking solution containing a secondary antibody to reveal TH (donkey anti-rabbit Alexa Fluor 594, Invitrogen A21207, lots 1890862 and 2145022 [1:400]; RRID: AB_141637). The slices were rinsed three times in PBS for 10 min and mounted on Colorfrost Plus (Fisher 1255017) with a medium with DAPI (Vectashield H-1200) or without DAPI (Vectashield H-1000), covered with a 1.5 type glass coverslip and stored at 4 °C before observation.

RNAscope. To detect the *ZsGreen* and *Vglut2* (also called Slc17a6) mRNAs in coronal brain slices, we used the Advanced Cell Diagnostics RNAscope Multiplex Fluorescent Reagent Kit v2 Assay on fixed frozen tissue samples (ACD 323100-USM). All steps were carried out at room temperature unless stated otherwise. Mice were anesthetized with isoflurane (5% and 2.5 L/min) and transcardially perfused with 50 mL PBS, followed by 50 mL PBS solution containing 4% (weight/volume) of PFA. Brains were extracted and snap frozen on dry ice and sectioned at −20 °C in 15-μm thick coronal slices using a cryostat (Leica CM 1860 UV) and mounted onto Colorfrost Plus glass slides (Fisher 1255017). Sections were air dried during 2 h at −20 °C, washed in PBS during 5 min, and baked during 30 min at 60 °C in a HybEZ II oven (ACD 321721). Sections were then dehydrated in increasing concentrations of ethanol (50, 70, 100, and 100%, 5 min each), treated with hydrogen peroxide during 10 min (ACD 322381, lot 2011534) with RNAscope 1× Target Retrieval Agent during 5 min (ACS 322000, lot 2011356), and with protease III during 30 min in the oven at 40 °C (ACD 322381, lot 2011534). Sections were then treated during 2 h at 40 °C in the oven with an RNA hybridization antisense probe against ZsGreen-C1 (ACD 461251, lot 20296A) and another against mouse Slc17a6-C4 (i.e., Vglut2, ACD 319171-C4, and lot 21049B). After overnight incubation in a saline sodium citrate solution (175.3 g NaCl and 88.2 g sodium citrate in 1L of distilled water, pH = 7.0), C1 probe amplification was done using RNAscope Multiplex Fluorescent Detection Reagents v2 (ACD 323110, lot 2011351). C4 probe amplification was done with the RNAscope Multiplex Fluorescent Detection Reagents v2, with the addition of the HRP-C4 (ACD 323121, lot 2011711). C1 and C4 probes were revealed using Opal Dye 520 (Akoya Biosciences FP1487001KT, lot 201008031, and 1:150 or 1:1,500) and Opal Dye 690 (Akoya Biosciences FP1497001KT, lot 201008030, and 1:150 or 1:1,500). Sections were counterstained with DAPI (ACD 323108, lot 2011350), mounted with a ProLong Gold Antifade Mountant (Invitrogen P36930, lot 2305164), covered with a 1.5 type glass coverslip and stored at +4 °C before observation.

Microscopy. Brain sections were observed using a Zeiss AxioImager M2 microscope bundled with StereoInvestigator 2018 software (version 1.1, MBF Bioscience). To show the expression of ChR2-EYFP in the CnF, high-magnification (63×) photographs were taken using a Leica TCS SP8 nanoscope bundled with LASX software (Leica). Composite images were assembled using StereoInvestigator. The levels were uniformly adjusted in Photoshop CS6 (Adobe) to make all fluorophores visible and avoid pixel saturation, and digital images were merged.

Cell Counting. The procedure was as previously reported (51). To estimate the number of TH-positive cells in the SNc, for each animal, two coronal brain slices were photographed at 20× magnification with the epifluorescent microscope Zeiss AxioImager M2. On each side of the slice, a region of interest was traced over the photograph using ImageJ; its area was measured and the cells positive for TH were counted and expressed as the number of cells per surface unit (centimeters squared). Our criterion for cell count was a clear labeling of the cell body, as previously reported (51).

TH Optical Density. To estimate the density of the TH innervation in the striatum, measures of optical density of the TH-immunopositive signal was used (see, e.g., refs. 83 and 84). For each animal, two coronal sections at the level of the striatum were imaged using an epifluorescent microscope Zeiss AxioImager M2. Using ImageJ, regions of interest were drawn manually over the photographs to delineate the striatum. To estimate optical density in the regions of interest, the photographs were converted into a greyscale and compared to a calibrated greyscale taken from the ImageJ optical density calibration protocol (https://imagej.nih.gov/ij/docs/examples/calibration/) (see also ref. 83).

Statistical Analysis. Data are presented as mean ± SEM unless stated otherwise. No statistical method was used to predetermine sample sizes, which are similar to those used in the field (e.g., refs. 17 and 19). No randomization or blinding procedure was used. Statistical analysis was done using Sigma Plot 12.0. Parametric analyses were used when assumptions for normality and equal variance were respected, otherwise nonparametric analyses were used. Normality was assessed using the Shapiro–Wilk test. Equal variance was assessed using the Levene test. To compare the means between two dependent groups, a parametric two-tailed paired *t* test was used. To compare the means between two independent groups, a two-tailed *t* test or a nonparametric Mann–Whitney rank sum test was used. For more than two dependent groups, a parametric one-way ANOVA for repeated measures or a nonparametric Friedman ANOVA for repeated measures on ranks were used. ANOVAs were followed by a Student–Newman–Keuls post hoc test for multiple comparisons between groups. Linear and sigmoidal regressions between variables, their significance, and the 95% CIs were calculated using Sigma Plot 12.0. Relations between variables were tested using the Spearman rank order correlation. Statistical differences were assumed to be significant when $P < 0.05$.

Data Availability. Datasets have been deposited in Figshare (https://doi.org/10.6084/m9.figshare.15506028.v1). All other study data are included in the main text.

ACKNOWLEDGMENTS. We thank Jean Lainé for his technical assistance with the microscopy platform and Florian Bentzinger for providing access to the genotyping equipment. P.S. is the holder of the Canada Research Chair Tier 1 in the Neurophysiopharmacology of Chronic Pain. This work was supported by the Canadian Institutes of Health Research (407083 to D.R.), the Fonds de la Recherche Québec (Junior 1 Awards 34920 and 36772 to D.R. and Junior 2 Award 297238 to D.R.), the Natural Sciences and Engineering Research Council of Canada (RGPIN-2017-05522 and RTI-2019-00628 to D.R.), the Canada Foundation for Innovation (39344 to D.R.), the Centre d'Excellence en Neurosciences de l'Université de Sherbrooke (pilot project grant to D.R.), the Centre de Recherche du Centre Hospitalier Universitaire de Sherbrooke (start-up funding and programme d'aide financière interne grant to D.R.), and the Faculté de médecine et des sciences de la santé (start-up funding to D.R.).

1. B. R. Bloem, J. M. Hausdorff, J. E. Visser, N. Giladi, Falls and freezing of gait in Parkinson's disease: A review of two interconnected, episodic phenomena. *Mov. Disord.* **19**, 871–884 (2004).
2. E. C. Hirsch, A. M. Graybiel, C. Duyckaerts, F. Javoy-Agid, Neuronal loss in the pedunculopontine tegmental nucleus in Parkinson disease and in progressive supranuclear palsy. *Proc. Natl. Acad. Sci. U.S.A.* **84**, 5976–5980 (1987).
3. R. M. Zweig *et al.*, Loss of pedunculopontine neurons in progressive supranuclear palsy. *Ann. Neurol.* **22**, 18–25 (1987).
4. K. Jellinger, The pedunculopontine nucleus in Parkinson's disease, progressive supranuclear palsy and Alzheimer's disease. *J. Neurol. Neurosurg. Psychiatry* **51**, 540–543 (1988).
5. J. O. Rinne, S. Y. Ma, M. S. Lee, Y. Collan, M. Röyttä, Loss of cholinergic neurons in the pedunculopontine nucleus in Parkinson's disease is related to disability of the patients. *Parkinsonism Relat. Disord.* **14**, 553–557 (2008).
6. A. Demain *et al.*, High-level gait and balance disorders in the elderly: A midbrain disease? *J. Neurol.* **261**, 196–206 (2014).
7. C. Karachi *et al.*, Cholinergic mesencephalic neurons are involved in gait and postural disorders in Parkinson disease. *J. Clin. Invest.* **120**, 2745–2754 (2010).
8. D. Ryczko, R. Dubuc, Dopamine and the brainstem locomotor networks: From lamprey to human. *Front. Neurosci.* **11**, 295 (2017).
9. M. G. Sirota, G. V. Di Prisco, R. Dubuc, Stimulation of the mesencephalic locomotor region elicits controlled swimming in semi-intact lampreys. *Eur. J. Neurosci.* **12**, 4081–4092 (2000).
10. F. Brocard *et al.*, The transformation of a unilateral locomotor command into a symmetrical bilateral activation in the brainstem. *J. Neurosci.* **30**, 523–533 (2010).
11. J.-M. Cabelguen, C. Bourcier-Lucas, R. Dubuc, Bimodal locomotion elicited by electrical stimulation of the midbrain in the salamander *Notophthalmus viridescens*. *J. Neurosci.* **23**, 2434–2439 (2003).
12. D. Ryczko, F. Auclair, J.-M. Cabelguen, R. Dubuc, The mesencephalic locomotor region sends a bilateral glutamatergic drive to hindbrain reticulospinal neurons in a tetrapod. *J. Comp. Neurol.* **524**, 1361–1383 (2016).
13. F. Bretzner, R. M. Brownstone, Lhx3-Chx10 reticulospinal neurons in locomotor circuits. *J. Neurosci.* **33**, 14681–14692 (2013).
14. A. M. Lee *et al.*, Identification of a brainstem circuit regulating visual cortical state in parallel with locomotion. *Neuron* **83**, 455–466 (2014).
15. T. K. Roseberry *et al.*, Cell-type-specific control of brainstem locomotor circuits by basal ganglia. *Cell* **164**, 526–537 (2016).
16. P. Capelli, C. Pivetta, M. Soledad Esposito, S. Arber, Locomotor speed control circuits in the caudal brainstem. *Nature* **551**, 373–377 (2017).
17. V. Caggiano *et al.*, Midbrain circuits that set locomotor speed and gait selection. *Nature* **553**, 455–460 (2018).
18. N. Josset *et al.*, Distinct contributions of mesencephalic locomotor region nuclei to locomotor control in the freely behaving mouse. *Curr. Biol.* **28**, 884–901.e3 (2018).
19. C. I. van der Zouwen *et al.*, Freely behaving mice can brake and turn during optogenetic stimulation of the mesencephalic locomotor region. *Front. Neural Circuits* **15**, 639900 (2021).
20. D. Ryczko, R. Dubuc, The multifunctional mesencephalic locomotor region. *Curr. Pharm. Des.* **19**, 4448–4470 (2013).
21. M. Stephenson-Jones, E. Samuelsson, J. Ericsson, B. Robertson, S. Grillner, Evolutionary conservation of the basal ganglia as a common vertebrate mechanism for action selection. *Curr. Biol.* **21**, 1081–1091 (2011).
22. A. V. Kravitz *et al.*, Regulation of parkinsonian motor behaviours by optogenetic control of basal ganglia circuitry. *Nature* **466**, 622–626 (2010).
23. D. Ryczko *et al.*, Forebrain dopamine neurons project down to a brainstem region controlling locomotion. *Proc. Natl. Acad. Sci. U.S.A.* **110**, E3235–E3242 (2013).
24. D. Ryczko *et al.*, A descending dopamine pathway conserved from basal vertebrates to mammals. *Proc. Natl. Acad. Sci. U.S.A.* **113**, E2440–E2449 (2016).
25. D. Ryczko *et al.*, Nigral glutamatergic neurons control the speed of locomotion. *J. Neurosci.* **37**, 9759–9770 (2017).
26. J. Pérez-Fernández, M. Stephenson-Jones, S. M. Suryanarayana, B. Robertson, S. Grillner, Evolutionarily conserved organization of the dopaminergic system in lamprey: SNc/VTA afferent and efferent connectivity and D2 receptor expression. *J. Comp. Neurol.* **522**, 3775–3794 (2014).
27. S. Sharma, L. H. Kim, K. A. Mayr, D. A. Elliott, P. J. Whelan, Parallel descending dopaminergic connectivity of A13 cells to the brainstem locomotor centers. *Sci. Rep.* **8**, 7972 (2018).
28. A.-S. Rolland *et al.*, Evidence for a dopaminergic innervation of the pedunculopontine nucleus in monkeys, and its drastic reduction after MPTP intoxication. *J. Neurochem.* **110**, 1321–1329 (2009).
29. J. M. Shine *et al.*, Exploring the cortical and subcortical functional magnetic resonance imaging changes associated with freezing in Parkinson's disease. *Brain* **136**, 1204–1215 (2013).
30. V. Fraix *et al.*, Pedunculopontine nucleus area oscillations during stance, stepping and freezing in Parkinson's disease. *PLoS One* **8**, e83919 (2013).
31. Š. Holiga *et al.*, Resting-state functional magnetic resonance imaging of the subthalamic microlesion and stimulation effects in Parkinson's disease: Indications of a principal role of the brainstem. *Neuroimage Clin.* **9**, 264–274 (2015).
32. E. J. Knight *et al.*, Motor and nonmotor circuitry activation induced by subthalamic nucleus deep brain stimulation in patients with Parkinson disease: Intraoperative functional magnetic resonance imaging for deep brain stimulation. *Mayo Clin. Proc.* **90**, 773–785 (2015).
33. P. H. Weiss *et al.*, Subthalamic nucleus stimulation improves parkinsonian gait via brainstem locomotor centers. *Mov. Disord.* **30**, 1121–1125 (2015).
34. S. Breit, R. Bouali-Benazzouz, A. L. Benabid, A. Benazzouz, Unilateral lesion of the nigrostriatal pathway induces an increase of neuronal activity of the pedunculopontine nucleus, which is reversed by the lesion of the subthalamic nucleus in the rat. *Eur. J. Neurosci.* **14**, 1833–1842 (2001).
35. B. Neagu *et al.*, Pedunculopontine nucleus evoked potentials from subthalamic nucleus stimulation in Parkinson's disease. *Exp. Neurol.* **250**, 221–227 (2013).
36. S. B. Sébille *et al.*, Normal and pathological neuronal distribution of the human mesencephalic locomotor region. *Mov. Disord.* **34**, 218–227 (2019).
37. O. Gavriliuc *et al.*, Clinical patterns of gait freezing in Parkinson's disease and their response to interventions: An observer-blinded study. *Parkinsonism Relat. Disord.* **80**, 175–180 (2020).
38. P. Plaha, S. S. Gill, Bilateral deep brain stimulation of the pedunculopontine nucleus for Parkinson's disease. *Neuroreport* **16**, 1883–1887 (2005).
39. C. Hamani *et al.*, Pedunculopontine nucleus region deep brain stimulation in Parkinson disease: Surgical anatomy and terminology. *Stereotact. Funct. Neurosurg.* **94**, 298–306 (2016).
40. C. Hamani *et al.*, Pedunculopontine nucleus region deep brain stimulation in Parkinson disease: Surgical techniques, side effects, and postoperative imaging. *Stereotact. Funct. Neurosurg.* **94**, 307–319 (2016).
41. S. J. Chang, I. Cajigas, I. Opris, J. D. Guest, B. R. Noga, Dissecting brainstem locomotor circuits: Converging evidence for cuneiform nucleus stimulation. *Front. Syst. Neurosci.* **14**, 64 (2020).
42. S. J. Chang *et al.*, Deep brain stimulation of midbrain locomotor circuits in the freely moving pig. *Brain Stimul.* **14**, 467–476 (2021).
43. L. Goetz *et al.*, Deep brain stimulation of the pedunculopontine nucleus area in Parkinson disease: MRI-based anatomoclinical correlations and optimal target. *Neurosurgery* **84**, 506–518 (2019).
44. D. Dautan *et al.*, Modulation of motor behavior by the mesencephalic locomotor region. *Cell Rep.*, **36**, 109594 (2021).
45. M. M. Carvalho *et al.*, A brainstem locomotor circuit drives the activity of speed cells in the medial entorhinal cortex. *Cell Rep.* **32**, 108123 (2020).
46. G. D. R. Watson *et al.*, Thalamic projections to the subthalamic nucleus contribute to movement initiation and rescue of parkinsonian symptoms. *Sci. Adv.* **7**, eabe9192 (2021).

47. L. Vong *et al.*, Leptin action on GABAergic neurons prevents obesity and reduces inhibitory tone to POMC neurons. *Neuron* **71**, 142–154 (2011).
48. O. Yizhar, L. E. Fenno, T. J. Davidson, M. Mogri, K. Deisseroth, Optogenetics in neural systems. *Neuron* **71**, 9–34 (2011).
49. I. Opris *et al.*, Activation of brainstem neurons during mesencephalic locomotor region-evoked locomotion in the cat. *Front. Syst. Neurosci.* **13**, 69 (2019).
50. D. Li *et al.*, Lack of evidence for vesicular glutamate transporter expression in mouse astrocytes. *J. Neurosci.* **33**, 4434–4455 (2013).
51. M. Fougère, C. I. van der Zouwen, J. Boutin, D. Ryczko, Heterogeneous expression of dopaminergic markers and Vglut2 in mouse mesodiencephalic dopaminergic nuclei A8-A13. *J. Comp. Neurol.* **529**, 1273–1292 (2021).
52. S. Duty, P. Jenner, Animal models of Parkinson's disease: A source of novel treatments and clues to the cause of the disease. *Br. J. Pharmacol.* **164**, 1357–1391 (2011).
53. W. Thevathasan *et al.*; Movement Disorders Society PPN DBS Working Groupin collaboration with the World Society for Stereotactic and Functional Neurosurgery, Pedunculopontine nucleus deep brain stimulation in Parkinson's disease: A clinical review. *Mov. Disord.* **33**, 10–20 (2018).
54. M. L. Shik, F. V. Severin, G. N. Orlovskiĭ, [Control of walking and running by means of electric stimulation of the midbrain]. *Biofizika* **11**, 659–666 (1966).
55. S. J. Chang *et al.*, Deep brain stimulation of the Cuneiform nucleus for levodopa-resistant freezing of gait in Parkinson's disease: Study protocol for a prospective, pilot trial. *Pilot Feasibility Stud.* **7**, 117 (2021).
56. S. J. Chang *et al.*, MR tractography-based targeting and physiological identification of the cuneiform nucleus for directional DBS in a Parkinson's disease patient with levodopa-resistant freezing of gait. *Front. Hum. Neurosci.* **15**, 676755 (2021).
57. J. S. Schor, A. B. Nelson, Multiple stimulation parameters influence efficacy of deep brain stimulation in parkinsonian mice. *J. Clin. Invest.* **129**, 3833–3838 (2019).
58. J. K. Trevathan *et al.*, Calcium imaging in freely-moving mice during electrical stimulation of deep brain structures. *J. Neural Eng.* **18**, 026008 (2021).
59. S. Valverde *et al.*, Deep brain stimulation-guided optogenetic rescue of parkinsonian symptoms. *Nat. Commun.* **11**, 2388 (2020).
60. L. C. Bachmann *et al.*, Deep brain stimulation of the midbrain locomotor region improves paretic hindlimb function after spinal cord injury in rats. *Sci. Transl. Med.* **5**, 208ra146 (2013).
61. G. Deuschl *et al.*; German Parkinson Study Group, Neurostimulation Section, A randomized trial of deep-brain stimulation for Parkinson's disease. *N. Engl. J. Med.* **355**, 896–908 (2006). Correction in: *N. Engl. J. Med.* **355**, 1289 (2006).
62. D. Su *et al.*, Frequency-dependent effects of subthalamic deep brain stimulation on motor symptoms in Parkinson's disease: A meta-analysis of controlled trials. *Sci. Rep.* **8**, 14456 (2018).
63. F. J. Urbano, V. Bisagno, S. Mahaffey, S.-H. Lee, E. Garcia-Rill, Class II histone deacetylases require P/Q-type Ca^{2+} channels and CaMKII to maintain gamma oscillations in the pedunculopontine nucleus. *Sci. Rep.* **8**, 13156 (2018).
64. V. Bisagno, M. A. Bernardi, S. Sanz Blasco, F. J. Urbano, E. Garcia-Rill, Differential effects of HDAC inhibitors on PPN oscillatory activity in vivo. *Neuropharmacology* **165**, 107922 (2020).
65. M. Ratner, Light-activated genetic therapy to treat blindness enters clinic. *Nat. Biotechnol.* **39**, 126–127 (2021). Correction in: *Nat. Biotechnol.* **39**, 387 (2021).
66. J. M. Cregg *et al.*, Brainstem neurons that command mammalian locomotor asymmetries. *Nat. Neurosci.* **23**, 730–740 (2020).
67. G. Usseglio, E. Gatier, A. Heuzé, C. Hérent, J. Bouvier, Control of orienting movements and locomotion by projection-defined subsets of brainstem V2a neurons. *Curr. Biol.* **30**, 4665–4681.e6 (2020).
68. M. Lemieux, F. Bretzner, Glutamatergic neurons of the gigantocellular reticular nucleus shape locomotor pattern and rhythm in the freely behaving mouse. *PLoS Biol.* **17**, e2003880 (2019).
69. K. R. Bailey, J. N. Crawley, "Anxiety-related behaviors in mice" in *Methods of Behavior Analysis in Neuroscience, Frontiers in Neuroscience*, J. J. Buccafusco, Ed. (CRC Press/Taylor & Francis, ed. 2, 2009).
70. J. Nonnekes *et al.*, Freezing of gait: A practical approach to management. *Lancet Neurol.* **14**, 768–778 (2015).
71. D. Servello, E. Zekaj, C. Saleh, C. Menghetti, M. Porta, Long-term follow-up of deep brain stimulation of peduncolopontine nucleus in progressive supranuclear palsy: Report of three cases. *Surg. Neurol. Int.* **5** (suppl. 8), S416–S420 (2014).
72. Y. Wen, B. Jiao, Y. Zhou, L. Shen, A systematic review and meta-analysis of deep brain stimulation for progressive supranuclear palsy. *Research Square* [Preprint] (2020). https:/doi.org/10.21203/rs.3.rs-122655/v1 (Accessed 17 August 2021).
73. L. Madisen *et al.*, A toolbox of Cre-dependent optogenetic transgenic mice for light-induced activation and silencing. *Nat. Neurosci.* **15**, 793–802 (2012).
74. S. L. Thiele, R. Warre, J. E. Nash, Development of a unilaterally-lesioned 6-OHDA mouse model of Parkinson's disease. *J. Vis. Exp.* **60**, 3234 (2012).
75. A. Mathis *et al.*, DeepLabCut: Markerless pose estimation of user-defined body parts with deep learning. *Nat. Neurosci.* **21**, 1281–1289 (2018).
76. T. Nath *et al.*, Using DeepLabCut for 3D markerless pose estimation across species and behaviors. *Nat. Protoc.* **14**, 2152–2176 (2019).
77. S. B. Hausmann, A. M. Vargas, A. Mathis, M. W. Mathis, Measuring and modeling the motor system with machine learning. *Curr. Opin. Neurobiol.* **70**, 11–23 (2021).
78. T. Garland Jr., T. T. Gleeson, B. A. Aronovitz, C. S. Richardson, M. R. Dohm, Maximal sprint speeds and muscle fiber composition of wild and laboratory house mice. *Physiol. Behav.* **58**, 869–876 (1995).
79. H. Leblond, M. L'Esperance, D. Orsal, S. Rossignol, Treadmill locomotion in the intact and spinal mouse. *J. Neurosci.* **23**, 11411–11419 (2003).
80. K. He, X. Zhang, S. Ren, J. Sun, "Deep Residual Learning for Image Recognition" in *2016 IEEE Conference on Computer Vision and Pattern Recognition (CVPR)* (IEEE, Las Vegas, NV, 2016), pp. 770–778.
81. E. Insafutdinov, L. Pishchulin, B. Andres, M. Andriluka, B. Schiele, DeeperCut: A deeper, stronger, and faster multi-person pose estimation model. *arXiv* [Preprint] (2016). https://arxiv.org/abs/1605.03170 (Accessed 27 November 2020).
82. K. Franklin, G. Paxinos, *The Mouse Brain in Stereotaxic Coordinates, Compact* (Elsevier, ed. 3, 2008).
83. L. L. Xavier *et al.*, A simple and fast densitometric method for the analysis of tyrosine hydroxylase immunoreactivity in the substantia nigra pars compacta and in the ventral tegmental area. *Brain Res. Brain Res. Protoc.* **16**, 58–64 (2005).
84. V. Perlbarg *et al.*, Alterations of the nigrostriatal pathway in a 6-OHDA rat model of Parkinson's disease evaluated with multimodal MRI. *PLoS One* **13**, e0202597 (2018).